

Analytical microscopy of iron-based superconducting materials

S.C. Speller¹, T. Mousavi¹, P. Dudin²

¹ Department of Materials, University of Oxford, Oxford, OX1 3PH, UK

² Diamond Light Source, Harwell Science and Innovation Campus, Didcot OX11 0DE, UK

Abstract

Inhomogeneity and phase separation in unconventional superconducting materials is a topic of increasing interest, as the competition between phases with different types of ordering is thought to play an important role in the emergence of the high temperature superconducting state. A wide range of experimental techniques are available for investigating the crystallography of these complex materials, however the majority are bulk probes. Here we briefly review some spatially resolved techniques that are being used to investigate phase separation in iron-based superconductors, with a focus on analytic Scanning Electron Microscopy techniques and synchrotron-based Photoelectron Microscopy.

1. Introduction

Interest in nanoscale phase separation in superconducting materials was sparked in 1992 when intrinsic electronic and lattice inhomogeneity was proposed as a key feature for the emergence of high temperature superconductivity [1]. The notion that competition between phases with charge ordering, spin ordering and superconductivity results in the formation of complex, heterogeneous structures, arranged as self-organised, fluctuating networks of “superstripes”, has grown in popularity, fuelled by experimental evidence taken from a wide range of cuprate superconductors [2, 3]. Intrinsic inhomogeneity resulting in phase separation is believed to be at the root of understanding the puzzling “pseudogap” state of underdoped cuprate superconductors above T_c [4]. It is found that in some regions of the material, Cooper pair formation occurs above the resistive transition temperature (T_c) as disconnected “puddles”, leading to an anomalous diamagnetic signal. As the material is cooled, these puddles grow in size and at T_c they connect together to form a percolative path through the material and macroscopic phase coherence emerges along with the resistive transition. Mesoscopic phase separation, on length scales between 1nm and 100 μ m, has also been found in the novel iron-based superconductors (see for example [5, 6]), and there have been recent reports of this kind of inhomogeneity occurring even in a conventional LTS superconductor [7].

1.1 Iron-based Superconductors

Since the discovery of superconductivity at 26K in F-doped LaFeAsO [8], a vast family of iron-based materials with different structures and chemical compositions have been found to exhibit superconductivity. These novel materials sparked great interest from the condensed matter physics community for several reasons, as discussed in detail in a recent review article by Kordyuk [9]. Firstly, the interplay between superconductivity and magnetism in these materials leads to rich and interesting physics. Secondly, the wide variety of compounds in this family promise hope of discovering the elusive mechanism of high temperature superconductivity, paving the way for discoveries of new materials with higher transition temperatures. Finally, the materials have much higher critical fields and more isotropic transport properties than the cuprate high temperature

superconductors, making them interesting for practical electrical power and magnet applications as well as for spintronics.

The highest recorded transition temperature in a bulk material at ambient pressure of 55K has been found in SmFeAsO, another member of the oxypnictide or '1111' family. However, it is challenging to grow large single crystals of these compounds, making them difficult to study experimentally. In contrast, the '122' family of iron arsenide compounds can be grown as large, high quality single crystals with a wide range of hole and electron doping levels. The hole-doped compound $\text{Ba}_{1-x}\text{K}_x\text{Fe}_2\text{As}_2$ has a critical temperature as high as 38K [10]. LiFeAs is the most studied material in the '111' system. This has a transition temperature of 18K and interestingly it is stoichiometric, not requiring impurity doping to produce the superconducting state [11]. However, it is highly reactive in air, making it a challenging material to study. The superconducting compound with the simplest '11' crystal structure is binary FeSe, consisting of stacked tetrahedrally co-ordinated FeSe layers with no spacing atoms between the layers [12]. Doping FeSe with Te results in an increase in T_c from 8K to a maximum of 14K in $\text{Fe}_{1+y}\text{Se}_{0.5}\text{Te}_{0.5}$ [13]. Incorporating alkali metal atoms or Tl atoms between the FeSe layers produces a family of compounds with crystal structures analogous to the iron arsenide 122 compounds. These materials are found to intrinsically phase separate into a superconducting phase with $T_c \sim 30\text{K}$ coexisting with extremely high Neel temperature ($>500\text{K}$) antiferromagnetic phase with ordered iron vacancies [14, 15]. It is also interesting that the Fermi surface of these alkali metal iron selenides are completely electron-like, which precludes the most popular $s\pm$ pairing scenario [16].

In many of these families of iron-based superconductors, static magnetism is found to coexist with superconductivity in certain regions of the phase diagram [9]. An important question to answer is whether they coexist microscopically, with the same conduction electrons being involved in both physical phenomena, or are there two spatially separated phases present. Microscopy techniques as local probes of structure, chemistry and electronic properties can play an important role in resolving this issue.

1.2 Overview of characterisation techniques

The fundamental (intrinsic) properties of iron-based superconductors have been studied using a range of characterisation techniques that average over relatively large volumes of material, requiring either single crystal or high quality powder samples. Bulk probes used to characterise iron-based superconductors include standard SQUID magnetometry, X-ray diffraction (XRD) [17], X-ray Absorption Spectroscopy (XANES [18, 19], EXFAS [20, 21]), neutron scattering [22, 23, 24], Muon-spin rotation [25, 26], Nuclear Magnetic Resonance (NMR) [27] and Mossbauer Spectroscopy [28]. In addition, Angle-resolved Photoelectron Spectroscopy (ARPES), a surface sensitive synchrotron technique, is increasingly employed for measuring the band-structure of occupied electronic states in the vicinity of the Fermi level [29, 30, 31, 32]. However, it was noted recently by Müller that techniques that probe real space and time are more useful for studying inhomogeneous fluctuations in high temperature superconductivity [3].

It is challenging to grow uniform crystals of most of these complex iron-based superconductors, therefore it is crucially important to analyse the homogeneity of the samples using spatially-resolved techniques to enable the standard bulk measurements to be interpreted properly. Since the

mesoscopic length-scales of interest range from $\sim 1\text{nm}$ to $\sim 100\mu\text{m}$, often even within one material, various different microscopy techniques need to be employed.

Scanning Tunnelling Microscopy (STM) is the most common local spectroscopic probe used in the study of iron-based superconducting materials [33]. This powerful technique can be used to image with atomic resolution by fixing the tip bias voltage, or as a spectroscopic probe measuring the local density of states as a function of energy by sweeping the bias voltage on the tip and measuring the tunnelling current. Quasiparticle interference (QPI) has also been imaged in iron-based superconductors to shed light on the complexity of pairing symmetry, as discussed in detail in the recent review article by Hoffman [33]. STM has also been used to investigate the multitude of Fe-vacancy-ordered superstructures that are found in $\text{K}_x\text{Fe}_{2-y}\text{Se}_2$ crystals [34]. However STM studies are limited to imaging very small regions and require conducting samples.

Analytic (Scanning) Transmission Electron Microscopy (S)TEM has also been employed by a number of research groups to perform high resolution studies on iron-based superconductors. Cantoni et al have used aberration-corrected STEM to measure the local Fe moment and Fe orbital occupancy in a range of different compounds [35]. State-of-the-art atomic resolution Electron Energy Loss Spectroscopy (EELS) experiments have been carried out in a STEM by a number of different research groups to investigate chemical inhomogeneity in a range of compounds including $\text{LaFeAsO}_{1-x}\text{F}_x$ [36] and $\text{Fe}_{1+y}\text{Te}_x\text{Se}_{1-x}$ [37]. In addition, Wang et al. have used lattice imaging in a TEM to investigate Fe vacancy ordering in $\text{K}_x\text{Fe}_{2-y}\text{Se}_2$ crystals [38]. However, these techniques rely on producing extremely thin samples without creating artefacts in the crystals under investigation.

Scanning nano-focussed X-ray diffraction studies using a synchrotron radiation source have also been used to investigate phase separation in intrinsically phase-separated $\text{K}_x\text{Fe}_{2-y}\text{Se}_2$ superconducting crystals [5]. These experiments can measure the absolute values of the lattice parameters, but despite the small lateral dimensions of the focussed probe ($300\times 300\text{ nm}^2$), the interaction depth is much larger than some of the microstructural features ($\sim 11\mu\text{m}$). More recently, scanning micro-focussed XRD (with a larger probe size of $2\times 2\mu\text{m}^2$) has been carried out on similar crystals as a function of temperature, showing the evolution of a third phase at the interface between the superconducting and antiferromagnetic phases already discussed [39].

There are also several techniques for measuring the local magnetic properties of a material from the stray field produced in the vicinity of the surface of the sample. These include scanning SQUID microscopy, scanning Hall Probe microscopy (SHPM) and Magnetic Force Microscopy (MFM), and these have been reviewed in detail by Bending [40]. Park et al. has carried out MFM studies on slightly under-doped $\text{Ba}_{1-x}\text{K}_x\text{Fe}_2\text{As}_2$ single crystals, showing mesoscopic phase separation between a magnetically ordered phase and a non-magnetic phase in domains of $\sim 65\text{nm}$ [41]. Scanning SQUID microscopy has a lower spatial resolution than MFM, but a higher field sensitivity. Kalisky et al. has used a scanning SQUID with a $4\mu\text{m}$ pick-up loop to image ordered stripe structures in Co-doped $\text{Ba}_x\text{Fe}_2\text{As}_2$ crystals [42].

The remainder of this paper gives an overview of some of the different analytical microscopy techniques that we have used in Oxford to investigate phase separation and inhomogeneity in iron-based superconductors. It is not intended to be an exhaustive review, instead highlighting some key examples from our own recent experimental work.

2. Scanning Electron Microscopy

Modern scanning electron microscopes are powerful instrumental platforms that offer imaging resolutions down to 1-2 nm combined with the detection of a wide range of different signals, including secondary electrons, backscattered electrons and X-rays.

2.1 High-resolution Backscattered Electron Diffraction (HR-EBSD)

Backscattered electrons, inelastically scattered incident electrons, can be used to study the local structure and orientation of crystalline samples. The backscattered electrons are Bragg diffracted by the top 10-20nm of the crystal as they exit the sample, producing a diffraction pattern on a phosphor screen which is captured by a CCD camera (fig. 1). The Kikuchi bands on the EBSD pattern can be indexed if the structural parameters of the material are known, and from their positions on the screen, the local crystallographic orientation of the sample can be deduced. By scanning the electron beam and collecting and indexing patterns from each pixel, crystallographic orientation maps can be generated. However, it is also possible to obtain more detailed information from the EBSD patterns in single crystalline materials. Small lattice distortions across the sample result in small shifts in the positions of the bands. Using image correlation techniques described in detail by Wilkinson et al. [43], it is possible to extract the lattice displacement of each pixel relative to a reference position in the sample. If the elastic properties of the material are known, and the assumption that the deformation is under plane stress conditions, it is possible to calculate all the components of the strain tensor at each point. This is known as the high-resolution (HR) EBSD technique and has been mainly used to date for strain mapping in aerospace alloys with a precision of $\sim 10^{-4}$ and spatial resolution of $< 100\text{nm}$.

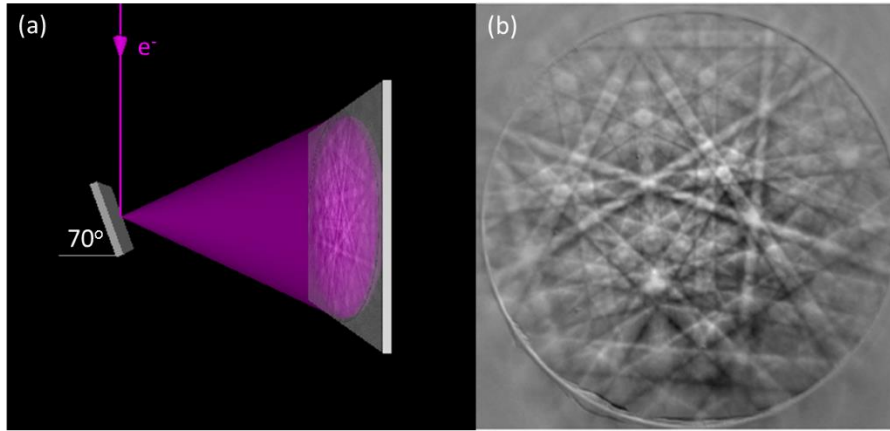


Figure 1: (a) Schematic diagram of the EBSD technique and (b) an example of an electron channelling pattern from a CaFe_2As_2 crystal.

In our work, we have applied this HR-EBSD technique to measure variations in unit cell anisotropy (c/a ratio) in single crystal samples of $\text{Fe}(\text{Se},\text{Te})$ and $\text{A}_x\text{Fe}_{2-y}\text{Se}_2$ superconductors (fig 2). For this application it is not necessary to make assumptions about the stress state or mechanical properties of the crystal, since they can be calculated directly from the lattice displacement data [44]. Figure 2(a) shows an HR-EBSD map of a single crystal of $\text{Fe}_{0.25}\text{Te}_{0.75}$ which exhibits a superconducting transition temperature of 10.5K co-existing with magnetic order, showing that it has significant structural inhomogeneity [44]. This is compared with a second similar crystal which displays only magnetic ordering (no superconductivity) and is much more homogeneous (fig 2(b)), providing direct imaging evidence that phase separation occurs in this material, with one phase being

superconducting and the other magnetic. This phase separation scenario is more pronounced in iron selenide materials with alkali metals incorporated between the FeSe layers, such as the $\text{Cs}_x\text{Fe}_{2-y}\text{Se}_2$ sample shown in figure 2(c). In this case it is found that the crystal phase separates forming a network of plate-type structures with high c/a ratio (red) aligned along the crystallographic [110] direction within a majority phase (matrix) with lower c/a ratio (yellow) [6]. Taken in relation with other experimental data we infer that the plate-shaped features, which make up about 10% by area, are the phase which becomes superconducting below $\sim 30\text{K}$, whereas the matrix is an antiferromagnetic insulator.

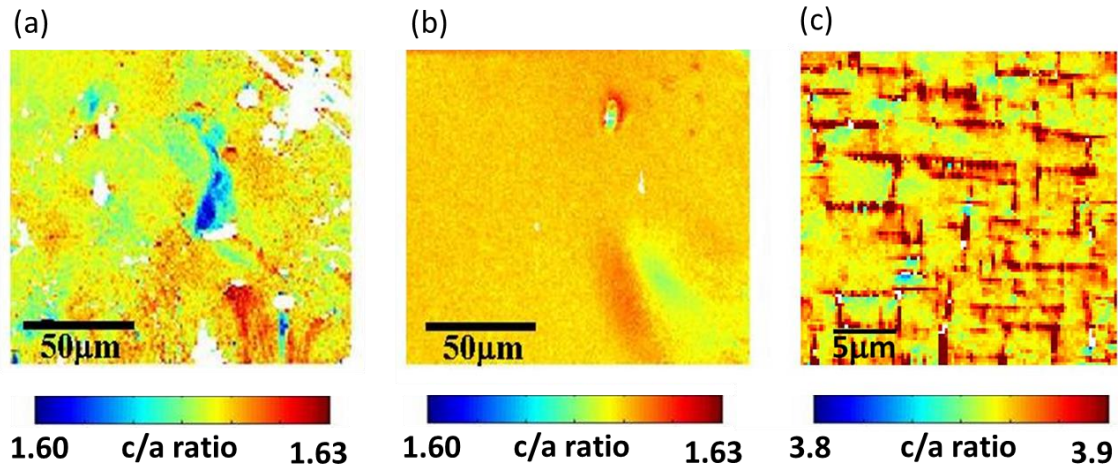


Figure 2: HR-EBSD maps showing spatial variation in c/a ratio in (a) $\text{Fe}_{0.95}\text{Se}_{0.25}\text{Te}_{0.75}$ (b) $\text{Fe}_{1.07}\text{Se}_{0.25}\text{Te}_{0.75}$ (c) $\text{Cs}_x\text{Fe}_{2-y}\text{Se}_2$ taken using a JEOL JSM 6500 FEGSEM using a TSL EBSD system and CrossCourt v3 (BLG Productions) software. (a) and (b) are reproduced from [44].

The HR-EBSD technique has the advantage over scanning nano-focussed XRD of significantly better spatial resolution of 50-100nm depending on the material. HR-EBSD can also be carried out in transmission mode, with resolution as good as 10nm [45]. However, HR-EBSD only measures changes in lattice parameter anisotropy relative to a reference point rather than the absolute lattice parameters that can be measured using XRD techniques. For this reason, using HR-EBSD in combination with XRD techniques is a powerful methodology for studying structural variations with nano-scale resolution.

2.2 Energy Dispersive X-ray analysis (EDX)

Energy dispersive X-ray (EDX) spectra created by characteristic X-rays generated by the incident beam can be analysed using appropriate internal or external standards and corrections to obtain the local chemical composition of the sample [46]. Quantitative chemical analysis using EDX has to be performed carefully, and the error in absolute concentrations will be at least 1%. However, variations in the ratios of elements in a compound can be calculated with more confidence. The spatial resolution of EDX is generally large ($\sim 1\mu\text{m}$), but in modern microscopes with high intensity field emission electron guns and large area X-ray detectors, the accelerating voltage can be reduced to 5kV, reducing the depth from which emitted X-rays originate and consequently improving the spatial resolution substantially. Quantitative analysis for heavier elements may become more difficult because the higher energy K and L lines are no longer excited.

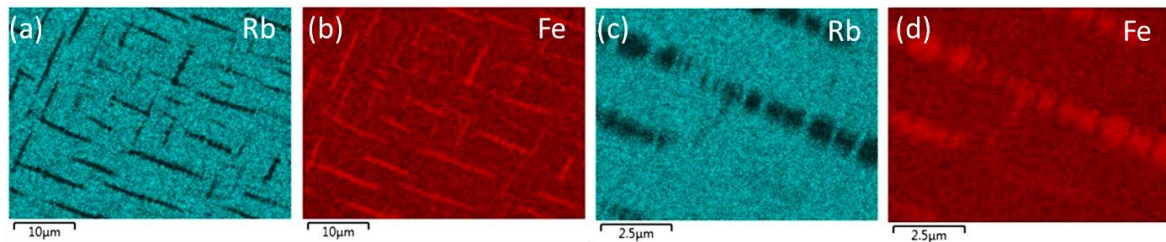


Figure 3: Elemental Rb and Fe EDX maps of $\text{Rb}_x\text{Fe}_{2-y}\text{Se}_2$ crystal taken at low magnification (a),(b) and high magnification (c),(d), using a Zeiss Merlin FEGSEM at 5kV. Reproduced from [47].

Figure 3 shows Fe and Se EDX maps taken at 5kV from a crystal of $\text{Rb}_x\text{Fe}_{2-y}\text{Se}_2$. Crystallographically aligned plate-like structures, similar in morphology to those shown in fig 2(c), are clearly seen to be rich in iron and deficient in Rb relative to the matrix. The Se maps are uniform. Higher voltage EDX analysis indicates that the matrix has a composition of $\sim\text{Rb}_{0.8}\text{Fe}_{1.6}\text{Se}_2$, with the features estimated to have composition closer to $\text{Rb}_{0.5}\text{Fe}_2\text{Se}_2$.

2.3 Scanning Transmission Electron Microscopy (STEM)

Recently it has become possible to carry out STEM experiments in some SEM instruments at voltages of 20-30kV, rather than at much higher voltages in a TEM. Using a high angle annular detector, we can obtain z-contrast images with spatial resolution well below 10nm [48]. STEM-in-SEM has advantages over TEM of lower accelerating voltages for beam sensitive samples, larger field-of-view, contrast enhancement and no projection lens producing chromatic aberration. Since thin foil specimens are used in these experiments, EDX microanalysis can be carried out at high accelerating voltages (30kV) to excite higher energy X-ray peaks without compromising on spatial resolution. Figure 4 shows STEM/EDX data from a $\text{Ca}_x\text{Fe}_2\text{As}_2$ single crystal grown from a FeAs-rich flux and annealed at 600°C [49]. Fig 4(a) shows the presence of a precipitate, less than 1μm long and 100nm wide, within a uniform matrix. Despite the nano-scale size of this precipitate, EDX mapping fig. 4(b-d) and linescans 4(e) clearly indicate that the precipitate is rich in both Fe and As, with a very low Ca content.

3. Photoelectron Microscopy (PEM)

Photoemission Spectroscopy (PES) works on the principle of illuminating a sample with high intensity photons (often soft X-rays) and detecting photoelectrons emitted from the surface. Spatial resolution can be achieved either by focusing the photon beam to a small spot size and scanning this across the sample or by illuminating a wider field of view and using electromagnetic lenses to form a full field image of the surface, as described in the following sections.

3.1 Scanning Photoelectron Microscopy (SPEM)

In the SPEM technique, incident photons are focussed into a spot using, for example, a Fresnel zone plate. In order to get sufficient intensity and energy resolution of the focussed photon beam, a synchrotron light source is required. In a typical SPEM experiment, the incident photon energy is kept constant and the energy of the emitted photoelectrons is measured. The binding energy of the photoelectrons (E_B) can be calculated from their measured kinetic energy (E_k) and the photon energy ($h\nu$), using the relation; $E_k = h\nu - E_B - \Phi$, where Φ is a work function of the material. Photons with energies between 10 eV and 10 keV efficiently excite atomic core levels, providing important chemical information about the sample. In addition the technique is surface sensitive, with low kinetic energy electrons (10-1000 eV) originating from a surface layer only few nm thick.

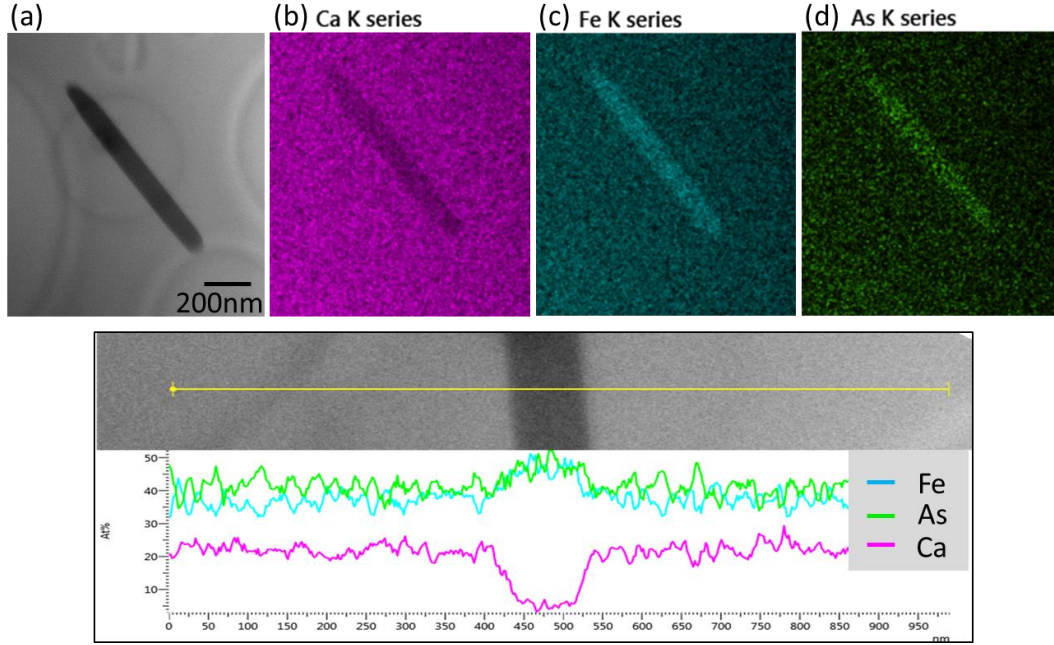


Figure 4: (a) STEM image of a FeAs precipitate in CaFe_2As_2 crystal grown from FeAs flux and annealed at 600oC. (b)-(d) EDX elemental maps from the same precipitate. (e) EDX linescan across the precipitate. All data taken using a thin foil specimen.

By measuring angular and energy distribution from small spot, it is possible to do nano- or micro-ARPES experiments to elucidate the local band structure (E-k dispersion) in the material. To achieve resolution in electron momentum, it is preferable to use low energy photons, and instrumentation with high resolution in energy and angle are required. To date, the practically usable energy resolution of the spatially resolved techniques is inferior to state-of-the-art classical ARPES instruments that use a larger beam size (20 - 50meV compared to <10meV, see, for example [50, 51]).

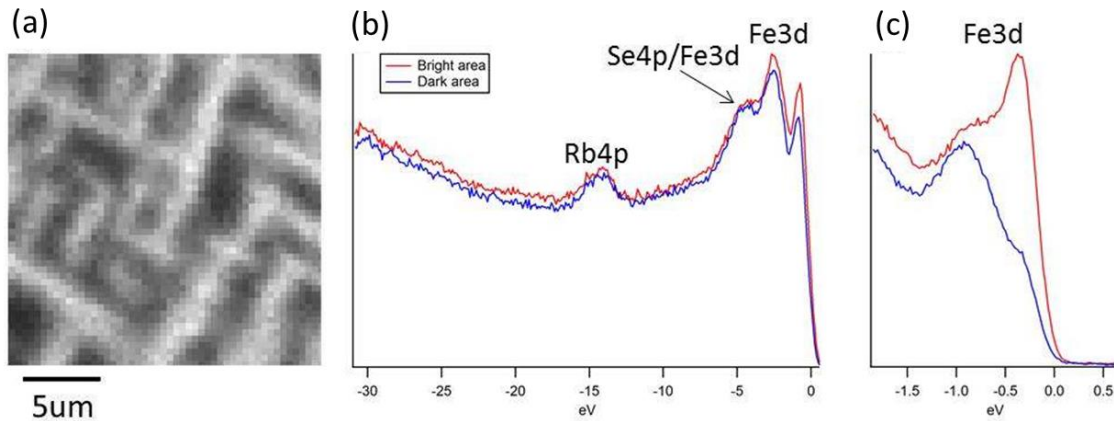


Figure 5: SPEM data from a $\text{Rb}_x\text{Fe}_{2-y}\text{Se}_2$ crystal taken on the SpectroMicroscopy beamline at Elettra synchrotron: (a) near-Fermi-level image, (b) survey spectrum and (c) spectrum near Fermi level. Reproduced from [47].

Figure 5 gives an example of a SPEM experiment carried out at the SpectroMicroscopy beamline at the Elettra Synchrotron on a phase-separated $\text{Rb}_x\text{Fe}_2\text{Se}_2$ crystal from the same batch shown in figure 3. The map in fig. 5(a) shows the variation in intensity of photoelectrons originating from electronic states within 1.15eV of the Fermi level (binding energies of -1.15eV to 0eV). A square network of

high intensity features can be seen, surrounded by a matrix with lower intensity. Spectra from bright (red/blue) and dark (blue/red) regions of the image are shown in fig. 5(b) and (c), indicating that the difference between the two regions is mainly the intensity of the lowest binding energy feature which is largely due to differences in occupation of the Fe3d orbitals, with the bright features being more metallic in nature compared to the dark regions. Results consistent with this interpretation have been found by another research group using the same beamline to investigate $K_x\text{Fe}_{2-y}\text{Se}_2$ crystals [52].

3.2 Photoelectron Emission Microscopy (PEEM)

The PEEM technique involves imaging the intensity of photoelectrons emitted as a result of absorption of ionising radiation (UV light or X-rays) using electromagnetic lenses to achieve magnification. The photoelectrons are accelerated towards the objective lens by a strong electric field generated by biasing the sample itself to 15-20kV. X-ray absorption spectra (XAS) can be measured from specific locations in the sample by taking a series of secondary electron PEEM images using different photon energies and reconstructing the photoelectron intensity as a function of energy from chosen regions of interest. In general this technique is used to probe the absorption spectra originating from the excitation of core electrons, while the SPEM techniques are more appropriate for photoemission from core levels or valence band. XAS data measured using PEEM not only gives information about the local chemistry and chemical environment of the atoms of interest, but by comparing XAS spectra taken with different X-ray polarisations, this technique can also be used to investigate dichroic effects resulting from magnetic ordering.

We have recently carried out PEEM experiments at the I06 beamline at Diamond Light Source on $\text{Rb}_x\text{Fe}_{2-y}\text{Se}_2$ crystals using light polarised in the linear horizontal (LH) and linear vertical (LV) configurations. Figure 6 (a) and (b) show the Fe XAS data reconstructed from the matrix phase and the minority phase, respectively. Whilst the XAS of the Fe L_3 and L_2 edges are qualitatively similar in both phases, there are subtle differences that are apparent in the polarisation averaged intensity images, such as the one shown in fig. 6(c). In general, it can be seen that the Fe content is higher in the minority phase, which is consistent with our previous analytical scanning electron microscopy results (fig. 3). There is an interesting difference in the XLD spectra from the two different phases; the matrix shows a dip and a peak at the L_3 edge, whereas this feature is absent in the minority phase. Since this XLD feature is a characteristic signature of antiferromagnetism [53], these results suggest that the antiferromagnetic ordering is present in the matrix but not in the minority phase [54].

4. Conclusions and future directions

Iron-based pnictide and chalcogenide compounds provide another family of materials, in addition to the cuprates, in which to study the low energy physics responsible for superconductivity at high temperatures. Inhomogeneity and mesoscale phase separation are believed to play an important role in the emergence of the superconducting state in unconventional superconductors. Therefore, in order to improve understanding of the mechanisms of high temperature superconductivity, a range of characterisation techniques sensitive to chemical, structural, electronic and magnetic inhomogeneity over different length-scales and time-scales are required to construct a complete picture of the landscape in which superconductivity arises. This paper has focussed on analytical microscopy techniques for direct visualisation of phase separation phenomena in iron-based

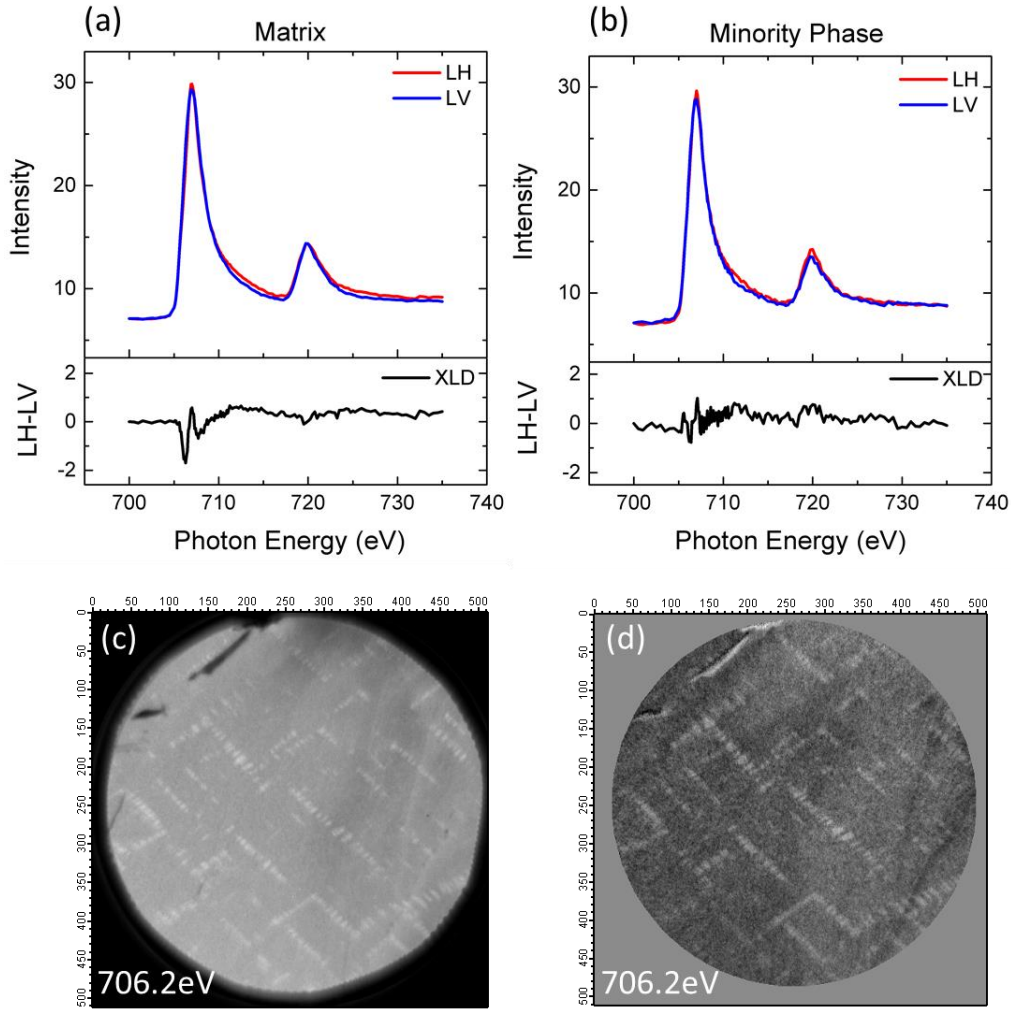


Figure 6: PEEM data of $\text{Rb}_x\text{Fe}_{2-y}\text{Se}_2$ crystal taken on I06 beamline at Diamond Light Source. Fe XAS spectra and XLD spectra from (a) matrix phase and (b) minority phase. Polarisation averaged (LH+LV) PEEM image (c) and XLD (LH-LV) image (d) are taken at 706.2 eV, at the minimum in the matrix XLD spectrum.

superconductors which we believe will play an increasingly important part in deciphering these complex materials. Most of the microscopy techniques discussed in detail here (with the exception of SPEM) were carried out at room temperature. However, since phase transformations and insulating/metallic crossover behaviour are often observed in the iron-based compounds on cooling below room temperature [39], the development of low temperature microscopy techniques to explore this microstructural evolution will be invaluable over the next few years.

Acknowledgements

The authors would like to acknowledge E. Pomjakushina and K. Conder (Paul Scherrer Institute) and A. Krzton-Maziopa (Warsaw University of Technology) for providing single crystal samples of $\text{Fe}(\text{Se},\text{Te})$ and $\text{A}_x\text{Fe}_{2-y}\text{Se}_2$ and P.C. Canfield and co-workers (Ames Lab.) for providing CaFe_2Se_2 single crystals. In addition, we would like to thank Alexey Barinov (Elettra Synchrotron) and Francesco Maccherozzi (Diamond Light Source) for their assistance with the SPEM and PEEM experiments, respectively.

References

- [1] K. A. Muller, G. Benedek, Phase separation in cuprate superconductors, Proceedings of the Workshop on Phase Separation in Cuprate Superconductors, (6-12 May 1992, Erice, Italy), Italy, 1992.
- [2] A. Bianconi, Superstripes, International Journal of Modern Physics B 14 (29-31), 2000, 3289.
- [3] K. A. Muller, The Unique Properties of Superconductivity in Cuprates, Journal of Superconductivity and Novel Magnetism 27, 2004, 2163.
- [4] V. Kresin, Y. N. Ovchinnikov, S. A. Wolf, Inhomogeneous Superconductivity and the Pseudogap State of Novel Superconductors, Physics Reports 431(5), 2006, 231.
- [5] A. Ricci, N. Poccia, G. Campi, B. Joseph, G. Arrighetti, L. Barba, M. Reynolds, M. Burghammer, H. Takeya, Y. Mizuguchi, Y. Takano, M. Colapietro, N. L. Saini, A. Bianconi, Nanoscale phase separation in the iron chalcogenide superconductor $\text{K}_{0.8}\text{Fe}_{1.6}\text{Se}_2$ as seen via scanning nanofocused x-ray diffraction, Physical Review B 84, 2011, 060511.
- [6] S. C. Speller, T. B. Britton, G. M. Hughes, A. Krzton-Maziopa, E. Pomjakushina, K. Conder, A. T. Boothroyd and C. R. M. Grovenor, Microstructural analysis of phase separation in iron chalcogenide superconductors, Superconductor Science and Technology 25, 2012, 084023.
- [7] A. Kamlapure, T. Das, S. C. Ganguli, J. B. Parmar, S. Bhattacharyya, P. Raychaudhuri, Emergence of nanoscale inhomogeneity in the superconducting state of a homogeneously disordered conventional superconductor, Science Reports 3, 2013, 2979.
- [8] Y. Kamihara, T. Watanabe, M. Hirano, H. Hosono, Journal of the American Chemical Society 130, 2008, 3296.
- [9] A. A. Kordyuk, Iron-based superconductors: Magnetism, superconductivity, and electronic structure, Low Temperature Physics 38, 2012, 888.
- [10] M. Rotter, M. Tegel, D. Johrendt, Superconductivity at 38 K in the Iron Arsenide $(\text{Ba}_{1-x}\text{K}_x)\text{Fe}_2\text{As}_2$, Physical Review Letters 101, 2008, 107006.
- [11] M. J. Pitcher, D. R. Parker, P. Adamson, S. J. C. Herkelrath, A. T. Boothroyd, R. M. Ibberson, M. Brunelli, S. J. Clarke, Structure and superconductivity of LiFeAs , Chemical Communications, 2008, 5918.
- [12] M. H. Fang, H. M. Pham, B. Qian, T. J. Liu, E. K. Vehstedt, Y. Liu, L. Spinu, Z. Q. Mao, Physical Review B 78, 2008, 224503.

- [13] K. W. Yeh, T. W. Huang, Y. L. Huang, T. K. Chen, F. C. Hsu, P. M. Wu, Y. C. Lee, Y. Y. Chu, C. L. Chen, J. W. Luo, D. C. Yan, M. K. Wu, Tellurium substitution effect on superconductivity of the α -phase iron selenide, *Europhysics Letters* 84, 2008, 37002.
- [14] V. Tsurkan, J. Deisenhofer, A. Gunther, H. A. Krug von Nidder, S. Widdman, A. Loidl, Anisotropic magnetism, superconductivity, and the phase diagram of $\text{Rb}_{1-x}\text{Fe}_{2-y}\text{Se}_2$, *Physical Review B* 84, 2011, 144520.
- [15] Y. J. Yan, M. Zhang, A. F. Wang, J. J. Ying, J. Y. Li, W. Qin, X. G. Luo, J. Q. Li, J. Hu, X. H. Chen, Electronic and magnetic phase diagram in $\text{K}_x\text{Fe}_{2-y}\text{Se}_2$ superconductors, *Scientific Reports* 2, 2012, 212.
- [16] P. J. Hirschfield, M. M. Korshunov, I. I. Mazin, Gap symmetry and structure of Fe-based superconductors, *Reports on Progress in Physics* 74, 2011, 124508.
- [17] T. Nomura, S. W. Kim, Y. Kamihara, M. Hirano, P. V. Sushko, K. Kato, M. Takata, A. L. Skyer, H. Hosono, Crystallographic phase transition and high- T_c superconductivity in LaFeAsO:F , *Superconductor Science and Technology* 21, 2008, 125028.
- [18] B. C. Chang, Y. B. You, T. J. Shiu, M. F. Tai, H. C. Ku, Y. Y. Hsu, L. Y. Jang, J. F. Lee, Z. Wei, K. Q. Ruan, X. G. Li, Angular dependence of x-ray absorption spectrum for field-aligned iron-based superconductors, *Physical Review B* 80, 2009, 165108.
- [19] W. Xu, A. Morcelli, B. Joseph, A. Iadecola, W. S. Chu, D. D. Gioachhino, A. Bianconi, Z. Wu, N. L. Saini, Local structural disorder in REFeAsO oxypnictides by RE L_3 edge XANES, *Journal of Physics: Condensed Matter* 22, 2010, 125701.
- [20] W. Chu, J. Cheng, S. Chu, T. Hu, A. Marcelli, X. Chen, Z. Wu, Iron Isotope Effect and Local Lattice Dynamics in the $(\text{Ba}, \text{K})\text{Fe}_2\text{As}_2$ Superconductor Studied by Temperature-Dependent EXAFS, *Scientific Reports* 3, 2013, 1750.
- [21] A. Iadecola, B. Joseph, M. Bendele, G. Aquilanti, H. Takeya, Y. Mizuguchi, Y. Takano, J. Mizokawa, N. L. Saini, Local structure response of phase separation and iron-vacancy order in $\text{K}_x\text{Fe}_{2-y}\text{Se}_2$ superconductor, *Physical Review B* 90, 2014, 174509.
- [22] D. S. Inosov, Spin fluctuations in iron pnictides and chalcogenides: from antiferromagnetism to superconductivity, *Comptes Rendus Physique*, doi:10.1016/j.crhy.2015.03.001
- [23] Q. Huang, Y. Qui, W. Bao, M. A. Green, J. W. Lynn, Y. C. Gasparoviz, T. Wu, G. Wu, X. H. Chen, Neutron-Diffraction Measurements of Magnetic Order and a Structural Transition in the Parent BaFe_2As_2 Compound of FeAs-Based High-Temperature Superconductors, *Physical Review Letters* 101, 2008, 257003.

- [24] V. Y. Pomjakushin, E. V. Pomjakushina, A. Krzton-Maziopa, K. Conder, D. Chernyshov, V. Svitlyk and A. Bosak, Intrinsic crystal phase separation in the antiferromagnetic superconductor $\text{Rb}_y\text{Fe}_{2-x}\text{Se}_2$: a diffraction study, *Journal of Physics: Condensed Matter* 24, 2012, 435701.
- [25] Z. Guguchia, Z. Shermadini, A. Amato, A. Maisuradie, A. Shengelaya, Z. Bukowski, H. Luetkens, R. Khasanov, J. Karpinski, H. Keller, Muon-spin rotation measurements of the magnetic penetration depth in the iron-based superconductor $\text{Ba}_{1-x}\text{Rb}_x\text{Fe}_2\text{As}_2$, *Physical Review B* 84, 2011, 094513.
- [26] C. Bernhard, C. N. Wang, L. Nuccio, L. Shultz, O. Zaharko, J. Larsen, C. Aristiabal, M. Willis, A. J. Drew, G. D. Varma, T. Wolf, C. Niedermayer, Muon spin rotation study of magnetism and superconductivity in $\text{Ba}(\text{Fe}_{1-x}\text{Co}_x)_2\text{As}_2$ single crystals, *Physical Review B* 86, 2012, 184509.
- [27] L. Ma, W. Q. Yu, Review of nuclear magnetic resonance studies on iron-based superconductors, *Chinese Physics B* 22, 2013, 087414.
- [28] A. Blachowski, K. Ruebenbauer, J. Zukrowski, Mössbauer spectroscopy of iron-based superconductors, *Annales UMCS Physica* 66, 2011, 125.
- [29] K. Terashima, Y. Sekiba, J. H. Bowen, K. Nakayama, T. Kawahara, T. Sato, P. Richard, Y.-M. Xu, L. J. Li, G. H. Cao, Z.-A. Xu, H. Ding and T. Takahashi, Fermi surface nesting induced strong pairing in iron-based superconductors, *Proceedings of the National Academy of Sciences* 106(18), 2009, 7330.
- [30] A. Tamai, A. Y. Ganin, E. Rozbicki, J. Basca, W. Meevasanna, P. D. C. King, M. Caffio, R. Schaub, S. Margadonna, K. Prassides, M. J. Rosseinsky, F. Baumberger, Strong Electron Correlations in the Normal State of the Iron-Based $\text{FeSe}_{0.42}\text{Te}_{0.58}$ Superconductor Observed by Angle-Resolved Photoemission Spectroscopy, *Physical Review Letters* 104(9), 2010, 097002.
- [31] C. Liu, G. D. Samolyuk, Y. Lee, N. Ni, T. Kondo, A. F. Santander-Syro, S. L. Bud'ko, J. L. McChesney, E. Rotenberg, T. Valla, A. V. Federov, P. C. Canfield, B. N. Herbon, A. Karminski, K-Doping Dependence of the Fermi Surface of the Iron Arsenic $\text{Ba}_{1-x}\text{K}_x\text{Fe}_2\text{As}_2$ Superconductor Using Angle-Resolved Photoemission Spectroscopy, *Physical Review Letters* 101, 2008, 177005.
- [32] S. V. Borisenko, V. B. Zabolotnyy, D. V. Evtushinsky, T. K. Kim, I. V. Morosov, N. Yaresko, A. A. Kordyuk, G. Behr, A. Vasiliev, R. Follath, B. Buchner, Superconductivity without Nesting in LiFeAs , *Physical Review Letters* 105(6), 2010, 067002.
- [33] J. Hoffman, Spectroscopic scanning tunneling microscopy insights into Fe-based superconductors, *Reports on Progress in Physics* 74, 2011, 124513.
- [34] W. Li, H. Ding, Z. Li, P. Deng, K. Chang, K. He, S. Ji, L. Wang, X. Ma, J.-P. Hu, X. Chen and Q.-K. Xue, KFe_2Se_2 is the Parent Compound of K-Doped Iron Selenide Superconductors, *Physical Review Letters* 109, 2012, 057003.

- [35] C. Cantoni, J. E. Mitchell, A. F. May, M. A. McGuire, J.-C. Idrobo, T. Berlijn, E. Dagotto, M. F. Chisholm, W. Zhou, S. J. Pennycook, A. S. Sefat, B. C. Sales, Orbital Occupancy and Charge Doping in Iron-Based Superconductors, *Advanced Materials* 26(35), 2014, 6193.
- [36] T. Tohei, T. Mizoguchi, H. Hiramatsu, Y. Kamihara, H. Hosono and Y. Ikukara, Direct imaging of doped fluorine in $\text{LaFeAsO}_{1-x}\text{F}_x$ superconductor by atomic scale spectroscopy, *Applied Physics Letters* 95, 2009, 193107.
- [37] H. Hu, J.-M. Zuo, J. Wen, Z. Xu, Z. Lin, Q. Li, G. G. W. K. Park, L. H. Greene, Phase separation in the iron chalcogenide superconductor $\text{Fe}_{1+y}\text{Te}_x\text{Se}_{1-x}$, *New Journal of Physics* 13, 2011, 053031.
- [38] Z. Wang, Y. J. Song, H. L. Shi, Z. W. Wang, Z. Chen, H. F. Tian, G. F. Chen, J. G. Guo, H. X. Yang, J. Q. Li, Microstructure and ordering of iron vacancies in the superconductor system $\text{K}_y\text{Fe}_x\text{Se}_2$ as seen via transmission electron microscopy, *Physical Review B* 83, 2011, 140505(R).
- [39] A. Ricci, N. Poccia, B. Joseph, D. Innocenti, G. Campi, A. Zozulya, F. Westermeier, A. Schavkan, F. Coneri, A. Bianconi, H. Takeya, Y. Mizuguchi, Y. Takano, T. Mizokawa, M. Sprung and N. L. Saini, Direct observation of nanoscale interface phase in the superconducting chalcogenide $\text{K}_x\text{Fe}_{2-y}\text{Se}_2$ with intrinsic phase separation, *Cond. Mat: arXiv* 1501, 2015, 06745.
- [40] S. J. Bending, Local magnetic probes of superconductors, *Advances in Physics* 48(4), 1999, 449.
- [41] J. T. Park, D. S. Inosov, C. Niedermayer, G. L. Sun, D. Haug, N. B. Christensen, R. Dinnebier, A. V. Boris, A. J. Drew, L. Schultz, T. Shapoval, U. Wolff, V. Neu, X. Yang, C. J. Lin, B. Keimer and V. Hinkov, Electronic Phase Separation in the Slightly Underdoped Iron Pnictide Superconductor $\text{Ba}_{1-x}\text{K}_x\text{Fe}_2\text{As}_2$, *Physical Review Letters* 102(11), 2009, 117006.
- [42] B. Kalisky, J. R. Kirtley, J. G. Analytis, J.-H. Chu, A. Valionis, I. R. Fisher and K. A. Moler, Stripes of increased diamagnetic susceptibility in underdoped superconducting $\text{Ba}(\text{Fe}_{1-x}\text{Co}_x)_2\text{As}_2$ single crystals: Evidence for an enhanced superfluid density at twin boundaries, *Physical Review B* 81, 2010, 184513.
- [43] A. Wilkinson, G. Meaden and D. Dingley, High-resolution elastic strain measurement from electron backscatter diffraction patterns: New levels of sensitivity, *Ultramicroscopy* 106, 2006, 307.
- [44] S. C. Speller, T. B. Britton, G. Hughes, S. Lozano-Perez, A. T. Boothroyd, E. Pomjakushina, K. Conder and C. R. M. Grovenor, High resolution characterisation of

microstructural evolution in $\text{Rb}_x\text{Fe}_{2-y}\text{Se}_2$ crystals on annealing, *Applied Physics Letters* 99, 2011, 192504.

- [45] R. R. Keller and R. H. Geiss, Transmission EBSD from 10 nm domains in a scanning electron microscope, *Journal of Microscopy* 245(3), 2012, 245.
- [46] D. E. Newbury and W. M. Ritchie, Is Scanning Electron Microscopy/Energy Dispersive X-ray Spectrometry (SEM/EDS) Quantitative?, *Scanning* 35, 2013, 141.
- [47] S. C. Speller, P. Dudin, S. Fitzgerald, G. M. Hughes, K. Kruska, T. B. Britton, A. Krzton-Maziopa, E. Pomjakushina, K. Conder, A. Barinov, C. R. M. Grovenor, High-resolution characterization of microstructural evolution in $\text{Rb}_x\text{Fe}_{2-y}\text{Se}_2$ crystals on annealing, *Physical Review B* 90, 2014, 024520.
- [48] C. A. Garcia-Negrete, M. C. Jimenez de Haro, J. Blasco, M. Soto, A. Fernandez, STEM-in-SEM high resolution imaging of gold nanoparticles and bivalve tissues in bioaccumulation experiments, *Analyst* 140(9), 2015, 2891.
- [49] S. Ran, S. Bud'ko, D. K. Pratt, A. Kreyssig, M. G. Kim, M. J. Kramer, D. H. Ryan, W. N. Rowan-Weetaluktuk, Y. Furokawa, B. Roy, A. I. Goldman, P. C. Canfield, Stabilization of an ambient-pressure collapsed tetragonal phase in CaFe_2As_2 and tuning of the orthorhombic-antiferromagnetic transition temperature by over 70 K via control of nanoscale precipitates, *Physical Review B* 83, 2011, 144517.
- [50] P. Dudin, P. Lacovig, C. Fava, E. Nicolini, A. Bianco, G. Cautero and B. A. Angle-resolved photoemission spectroscopy and imaging with a submicrometre probe at the spectromicroscopy-3.2L beamline of Elettra, *Journal Synchrotron Radiation* 17, 2010, 445.
- [51] J. Avila and M. C. Asensio, First NanoARPES User Facility Available at SOLEIL: An Innovative and Powerful Tool for Studying Advanced Materials, *Synchrotron Radiation News* 27(2), 2014, 24.
- [52] M. Bendele, A. Barinov, B. Joseph, D. Innocenti, A. Iadecola, A. Bianconi, H. Takeya, Y. Mizuguchi, T. Takano, T. Noji, T. Hatakeda, Y. Koike, M. Horio, A. Fujumori, D. Ootsuki, T. Mizokawa and N. L. Saini, Spectromicroscopy of electronic phase separation in $\text{K}_x\text{Fe}_{2-y}\text{Se}_2$ superconductor, *Scientific Reports* 4, 2014, 5592.
- [53] G. Van der Laan, Recent Advances in Circular and Linear X-ray Magnetic Dichroism: Experiment and Theory, *Synchrotron Radiation News* 26(6), 2013, 6.
- [54] S. Speller, T. Mousavi, P. Dudin and C. R. M. Grovenor, in preparation, 2015.

